ACS OMEGA

http://pubs.acs.org/journal/acsodf

Article

Microwave Heating Effect on Diamond Samples of Nitrogen-Vacancy Centers

Zheng Wang, Jintao Zhang,* Xiaojuan Feng,* and Li Xing

Cite This: *ACS Omega* 2022, 7, 31538−31543

Read Online

ACCESS | Metrics & More | Article Recommendations

ABSTRACT: Diamond samples of defects with negatively charged nitrogen-vacancy (NV) centers are promising solid-state spin sensors suitable for quantum information processing and highly sensitive measurements of magnetic, electric, and thermal fields at the nanoscale. A diamond defect with an NV center is unique for its robust temperature-dependent zero-field splitting D_{gs} of the triplet ground state. This property enables the optical readout of electron spin states through manipulation of the ground triplet state using microwave resonance with D_{gs} from 100 K to approximately 600 K. Thus, prohibiting D_{gs} from external thermal disturbances is crucial for an accurate measurement using NV-diamond sensors. Nevertheless, the external microwave field probably exerts a heating effect on the diamond sample of NV centers. To our knowledge, the microwave heating effect on the diamond samples of NV centers has yet to be quantitatively and systematically addressed. Our observation demonstrates the existence of a prominent microwave heating effect on the diamond samples of NV centers with the microwave irradiation in a continuous mode and some pulse sequence modes. The zero-field splitting D_{gs} is largely red-shifted by the temperature rises of the diamond samples. The effect will inevitably cause NV-diamond sensors to misread the true temperature of the target and disturb magnetic field detection by perturbing the spin precession of NV centers. Our observation demonstrates that such a phenomenon is negligible for the quantum lock-in XY8-N method.

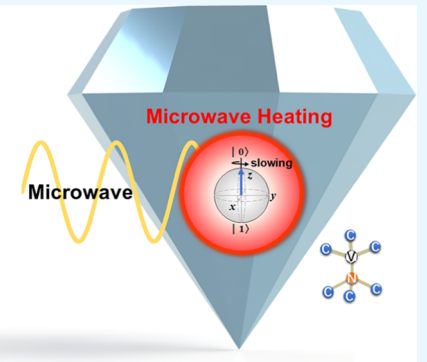

1. INTRODUCTION

The negatively charged nitrogen-vacancy (NV) center is a unique defect in diamond that is distinguished by its optical spin polarization and readout at room temperature.[1−5] This specific property makes NV center promising as solid-state spin sensors suitable for quantum physics studies and information processing,[6−11] nanoscale measurements of magnetic and electric fields,[12−16] and temperatures.[17−24] A spin projection split by a zero-field splitting D_{gs} enables the spin sublevels of a triplet ground state detectable by optically detected magnetic resonance (ODMR) in the continuous wave (CW) mode and the pulse wave sequence mode. In ODMR techniques, microwave resonances with D_{gs} enable manipulation of the spin state distribution to yield a difference in the optical emission intensity upon optical excitation. Thus, electron spin states are accessible by such manipulation. According to the literature,[25] the electronic spin Hamiltonian of the ground state spin $\hat{H}_{gs}$ is

$$\hat{H}_{gs} = \frac{1}{\hbar^2}(D_{gs} + d_{\parallel}\Pi_z)S_z^2 + \frac{\mu_B}{\hbar}\vec{S}\cdot\overline{g}\cdot\vec{B} - \frac{1}{\hbar^2}d_{\perp}\Pi_x(S_x^2 - S_y^2) + \frac{1}{\hbar^2}d_{\perp}\Pi_y(S_xS_y + S_yS_x) \quad (1)$$

where $\hbar$ stands for Planck's constant; D_{gs} is the zero-field splitting that is temperature-dependent; $d_{\parallel}$ and $d_{\perp}$denote the parallel and perpendicular electric dipole parameters, respectively; the total effective field $\vec{\Pi} = \vec{\sigma} + \vec{E}$ constitutes the electric field $\vec{E}$ and the effective strain field $\vec{\sigma}$; S_x, S_y, and S_z are the x, y, and z components of the spin operator, respectively; $\overline{g}$ is the Lande factor; μ_B is the Bohr magneton; and $\vec{B}$ is the external magnetic field.

Diamond is a semiconductor of multiple energy bands. A transmitting microwave interacts with the intrinsic fields in diamond, causing thermal energy dissipation in the sample.[26] We name such a formation of heat arising from dissipation of the microwave heating effect. Thus, microwave manipulation probably raises a perturbation to D_{gs}. Some researchers have been concerned with the microwave heating effect for the readout of the electron spin states of NV centers. Neumann et al.[27] and Wang et al.[14]varied the microwave power to find the specific irradiation that causes a nonobservable change in D_{gs}. Toylia et al.[17] argued that in the microwave pulse sequence mode, a practical microwave irradiation timescale is approx-

Received: July 5, 2022
Accepted: August 15, 2022
Published: August 24, 2022

imately 3 orders lower than the spin coherence times in a measurement. In that case, the heating effect is likely to be omitted. Xie et al.[28] intended to compensate for the disturbance of heating arising from coplanar waveguides. Lillie et al.[29] pointed out the observation of microwave heating by a thermistor installed on a superconductor Nb stage. To our knowledge, the microwave heating effect on the diamond samples of NV centers has yet to be quantitatively and systematically addressed.

Here, we demonstrate our quantitative observations on the microwave heating effect on diamond samples of NV centers. The tested samples were installed near room temperature. We studied the effect of typical continuous and pulsed sequence microwave irradiation at various powers. An infrared thermal imager and two thermocouples were applied for measuring thermal images and local temperatures on the surfaces of the diamond samples. We demonstrated the effect on the zero-field splitting D_{gs} of NV-diamond sensors.

2. EXPERIMENTAL SETUP

The experimental setup is shown in Figure 1a. The diamond samples of NV centers were made by chemical vapor

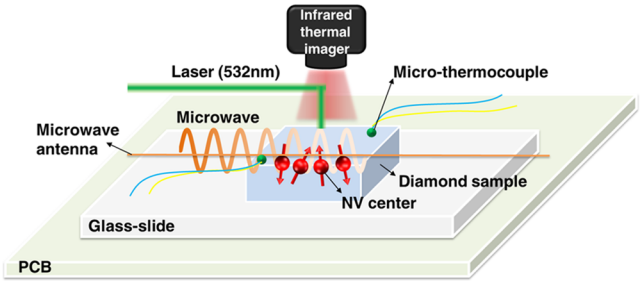

Figure 1. Schematic diagram of the experimental setup.

deposition (CVD) synthesis processes with dimensions of 2.6 mm × 2.6 mm × 0.3 mm from Element Six. The concentration of nitrogen in the sample was less than 1 ppm. The diamond samples were glued to glass slides with dimensions of 24 mm × 24 mm × 0.15 mm. The ensemble was fixed on a gold-plated printed circuit board (PCB). A thin straight wire antenna constituting a copper wire of 60 μm in diameter was closely attached to the upper surfaces of the diamond samples. We prepared two such ensembles, NV1 and NV2. The difference between the two ensembles lies in that NV1 was installed in an open environment without controlling temperature, and NV2 was accommodated in a temperature-controlled enclosure. The measurements with NV1 were implemented simultaneously by the infrared thermal imager and the thermocouples. The infrared thermal imager is a FLIR T650sc. The detector is 640 pixels × 480 pixels. The temperature sensitivity is better than 0.1 K at room temperature. The focal length is 22 mm. The spatial resolution is 0.41 mrad. The nominal accuracy is ±1 K. The camera can picture in discrete mode and continuous mode at a frequency of 30 Hz. The thermocouples are type K. They were diagonally attached to the upper surface of the diamond sample shown in Figure 1b. Their shields are 0.076 mm in outer diameter. Their reference junctions were properly set in an ice thermostat during measurements. The temperatures inside the enclosure accommodating NV2 were controlled within ±0.1 K surrounding the target temperature. To rule out the effect of temperature control on observing the observed microwave heating effect, we adopted the following control scheme where the controller is turned off when the temperature reaches the target temperature, but when the temperature is below the target temperature, the controller is turned on. Because the temperature-controlled enclosure hinders the optical path of the infrared thermal imager, the temperature of NV2 can only be measured with thermocouples.

We build a laser illuminating system to excite NV center and collect fluorescence to scan and locate the spin state of NV center better. We excite the NV center by 532 nm laser. After the laser is collimated, the acousto optic modulator (AOM) is used to modulate the optical path and control the switch of the laser. After passing through the AOM, the laser reaches the dichroic mirror and reflects on the front of the objective lens. Then, the laser focuses on the NV sample placed on the three-dimensional Physik Instrumente (PI) stage through the objective lens. After being excited, the NV sample generates fluorescence, returns along the original path, which passes through the dichroic mirror to the filter, and finally enters the multimode fiber through the fiber optic collimator. We collect fluorescence using a single photon counting modulator (SPCM) connected to data acquisition (DAQ). A vector signal generator (Rohde & Schwarz SMIQ04B), tuning from 300 kHz to 4.4 GHz at a resolution of 0.1 Hz, was used for microwave generation. The synthesized microwaves were transmitted through a radio frequency (RF) switch (Mini-Circuits ZASWA-2-50DRA+) and an amplifier (Mini-Circuits ZHL-16W-43-S+) of a specified range from 1.8 to 4 GHz to a straight wire antenna. We used a pulse generator (SpinCore PulseBlaster PBESR-PRO-500) with a specified pulse resolution and shortest pulse of 2 ns to generate pulse signals controlling the microwave RF switch. Based on the above devices, we simulated the microwave irradiation of a typical CW, Rabi pulse sequence, spin echo sequence, and XY8-10 pulse sequence and studied the microwave heating effect on the ground electron triplet spin state. All of the measurements reported here were implemented at zero-field splitting frequency near room temperature.

3. RESULT AND DISCUSSION

We first investigated the heating effects of the NV1 sample under continuous microwave irradiation of −13, −20, and −30 dBm. The duration of each irradiation was 60 s to simulate the general CW-ODMR process. The FLIR T650sc was operated in continuous image mode. A significant microwave heating effect was recorded in the infrared images. The temperature of the sample is related to microwave irradiation. We selected infrared images under −20 dBm microwave irradiation for the demonstration in Figure 2a. The diamond sample was observed in thermal equilibrium with the substrate and PCB before the onset of irradiation. After irradiation begins, the temperature rises rapidly in the diamond sample, while the temperature increase of the substrate is limited, and the temperature rise of PCB is hardly observed. The thermal image shows a circular diffusion distribution and the hottest spots are present in the center of the diamond sample. Extracting the real surface temperature of the sample using a radiation thermometer depends on accurately knowing the sample surface emissivity at the corresponding wavelength. However, accurate information on the actual emissivity of the diamond sample is unknown. We applied the instrument's default emissivity when operating the FLIR. Thus, the FLIR T650sc

https://doi.org/10.1021/acsomega.2c04232
ACS Omega 2022, 7, 31538−31543

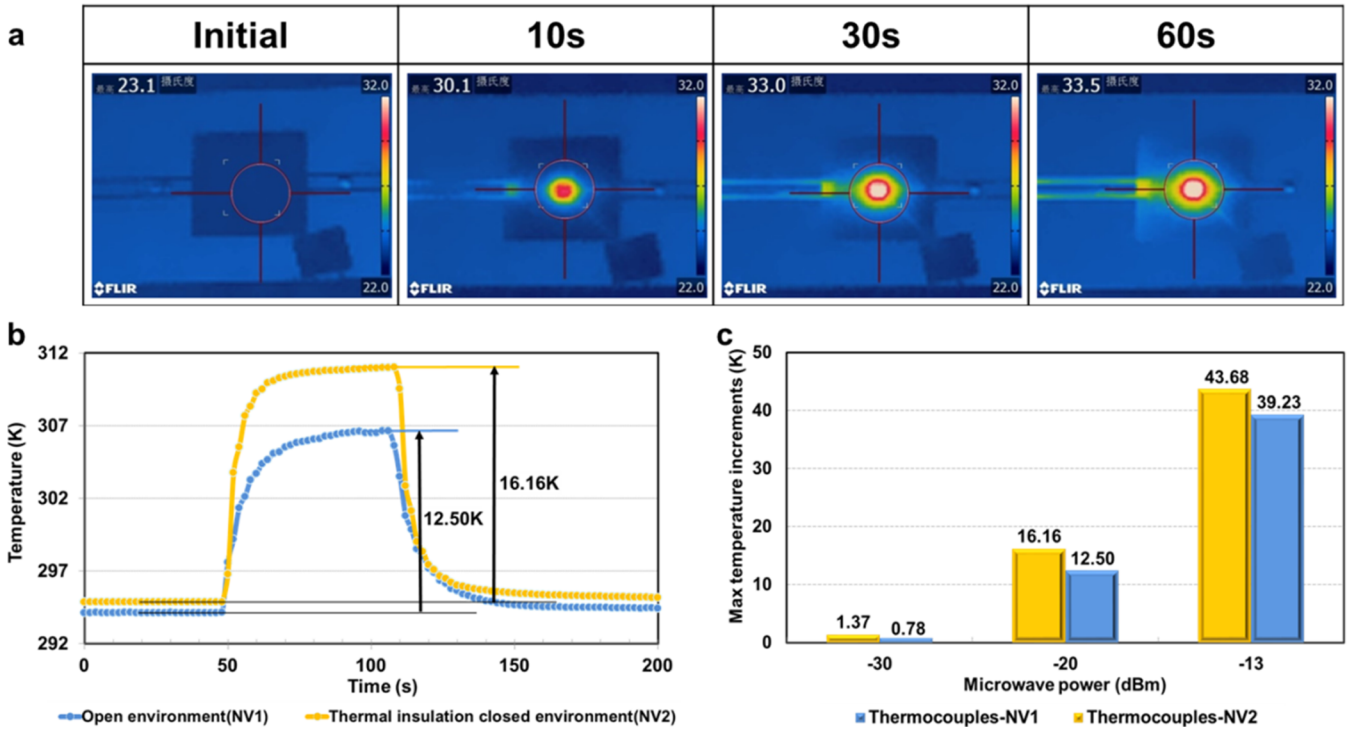

Figure 2. Temperature spectra for CW-ODMR. (a) Thermal images for NV1 upon irradiation at −20 dBm. (b) Temperature spectra for NV1 and NV2 upon microwave irradiation of −20 dBm. (c) Maximum histograms of the temperature rise at all microwave irradiation powers of NV1 and NV2.

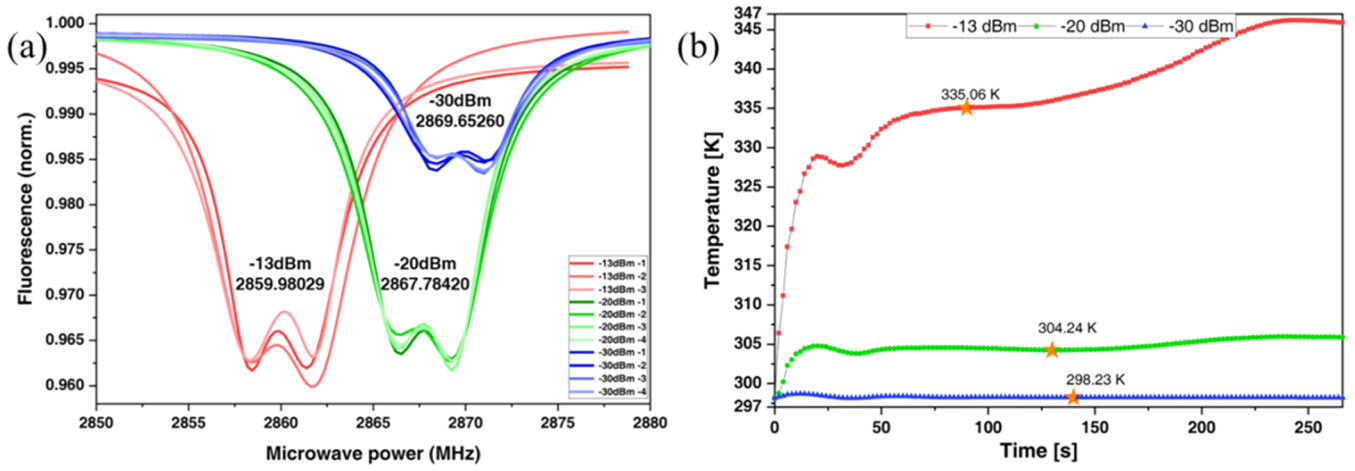

Figure 3. CW-ODMR spectrum and temperature variation diagram. (a) Zero-field ODMR spectra. (b) Temperature spectra for CW-ODMR.

readings are nominal, but these images correctly record the relative thermal tone on the surface of the NV1 diamond sample, reflecting the temperature distribution.

Due to the different positions of the two thermocouples, the measured thermal effects caused by microwave radiation are different. In all measurements, we took the average of the two thermocouple readings as a quantitative measurement of the sample surface temperature. In Figure 2b, we plot the time dependence of the temperatures measured under −20 dBm microwave irradiation for NV1 and NV2. Both relations are quite similar. The microwave heating effect is evident in both cases. The effect is stronger for NV2. The maximum rise rate is 3.48 $K{\cdot}s^{-1}$ for NV2 and 1.73 $K{\cdot}s^{-1}$ for NV1. The total temperature increment of NV2 is 16.16 K, and that of NV1 is 12.5 K. The samples were rapidly heated during the first 10 s of microwave irradiation, with NV2 and NV1 increasing at temperatures of 13.48 and 9.14 K. The subsequent temperature rise rate slowed significantly. Once the microwave irradiation is turned off, the sample rapidly loses its temperature in the first 10 s and then asymptotically approaches thermal equilibrium. We plot the maximum histograms of the temperature rise at all microwave irradiation powers of NV1 and NV2 in Figure 2c. The histograms show that the microwave heating effect is monotonically related to the microwave irradiation power. The maximum increment caused by −30 dBm irradiation was 1 order smaller than the maximum increment caused by −20 dBm irradiation. The maximum increment caused by −13 dBm can be as high as 312.38 and 316.83 K, respectively. Such an increment much exceeds the ambient temperature of NV1 and NV2.

https://doi.org/10.1021/acsomega.2c04232
ACS Omega 2022, 7, 31538−31543

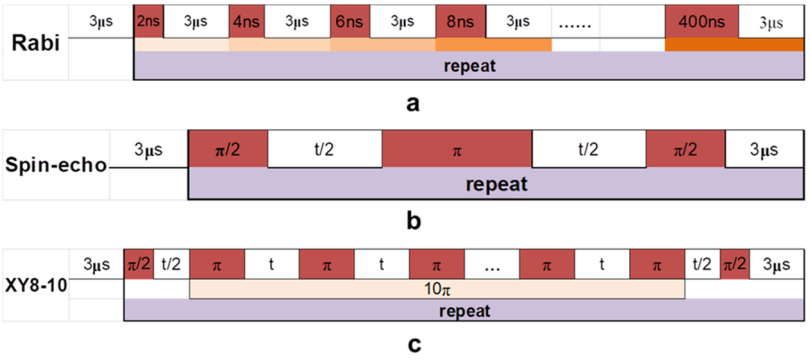

Figure 4. Pulse sequences. The sequence spares 3 μs before conducting an optical readout. (a) Rabi sequence. The microwave time increased 200 times in 2 ns steps. (b) Spin echo sequence. The $\pi/2$ pulse has a width of 50 ns spaced by the free evolution time (t) of 240 μs. (c) Quantum lock-in XY8-10 sequence. The $\pi/2$ pulse has a width of 50 ns spaced by the free evolution time (t) in 60 μs.

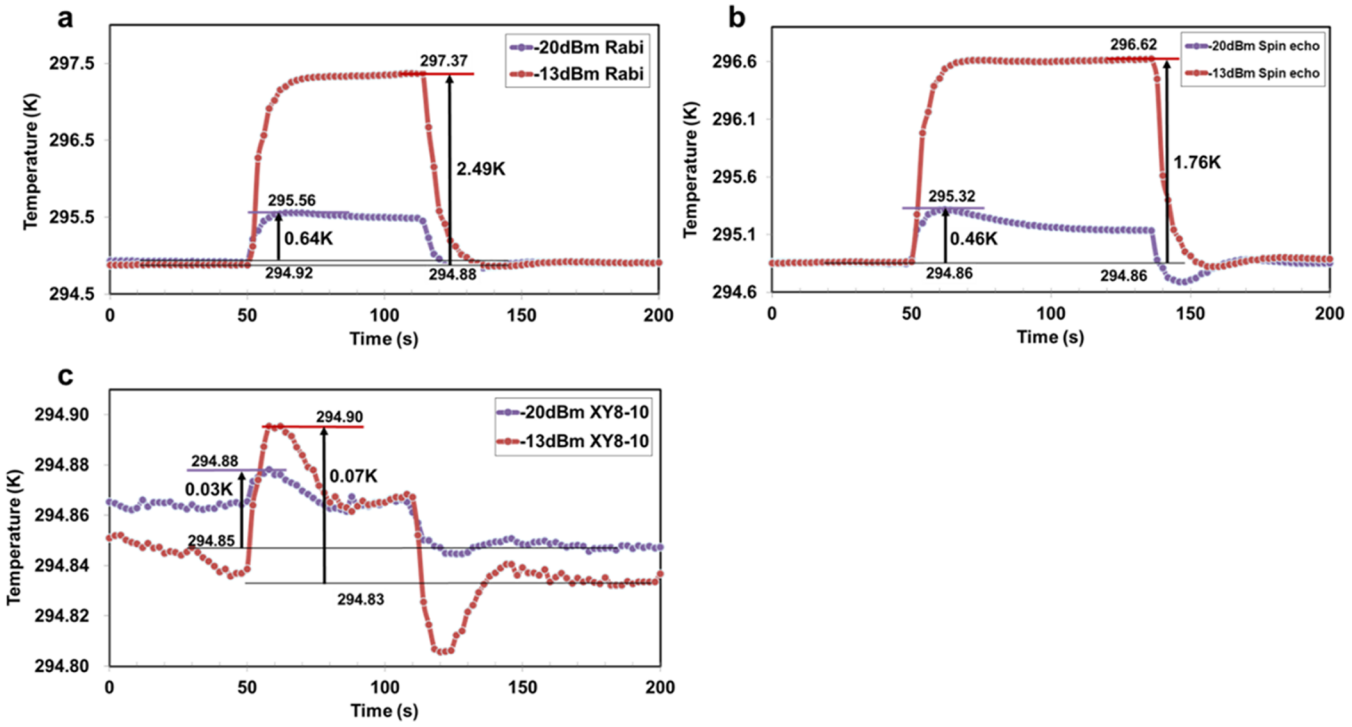

Figure 5. Temperature spectra by pulse microwave sequences under irradiation of −13 and −20 dBm. (a) Rabi sequence. (b) Spin echo. (c) Quantum lock-in XY8-10.

We further studied the microwave heating effect on the zero-field splitting D_{gs} of the NV-diamond sensors using CW-ODMR for NV2. To decouple a possible laser heating effect from our studied microwave heating effect, we kept the laser switching on before the microwave manipulation of the triplet ground state. By such a scheme, the effect of microwave irradiation will be independently identified. We observed the zero-field ODMR profiles of the electron spin ground state at the microwave irradiation of −13, −20, and −30 dBm, respectively. We carried out the observation at 298.15 K and maintained the temperature fluctuations of the samples within 10 mK for at least 10 minutes. We used the thermocouples shown in Figure 1 to measure the temporal temperatures on the diamond sample exposed to microwave irradiation. The microwave swept in the band from 2850 to 2890 MHz at a step of 0.2 MHz. The measurements were repeated three times for the microwave irradiation power of −13 dBm, and four times for −20 and −30 dBm. We fitted the profiles using the Lorentz method (Figure 3a). The center frequencies of the profiles at −30, −20, and −13 dBm were averaged to give the mean of 2869.65260, 2867.78420, and 2859.98029 MHz, respectively. The profiles show that the center frequency consistently shows redshift with increasing microwave irradiation power. Acosta, et al.[30] had pointed out that such redshift accompanies with the increase of the temperature detected by an NV-diamond sensor. We conclude that increasing the microwave irradiation power increases the temperature of the diamond sample accommodating the NV centers. We plotted in Figure 3b the dependence of the temperature of the diamond sample on the microwave irradiation power. We find that there was a rapid rise in temperature at the initial stage of turning on the microwave. The temperature rise acquired by the thermocouples at the central frequency D_{gs} was 0.08, 6.09, and 36.91 K at −30, −20, and −13 dBm, respectively. The result is compatible with that shown in Figure 2c. The experiment based on CW-ODMR confirms that, under the continuous

https://doi.org/10.1021/acsomega.2c04232
ACS Omega 2022, 7, 31538−31543

microwave irradiation at −13 and −20 dBm, notable microwave heating effect occurs, even in the case of the control of ambient temperatures.

We investigated the microwave heating effect on pulse microwave sequences. Our study mainly focused on NV2 with −13 and −20 dBm microwave irradiation. First, we investigated the microwave heating effect under microwave irradiation using a general Rabi oscillation. The Rabi pulse sequence is shown in Figure 4a, a sequence consisting of a series of pulses. The initial pulse was 2 ns wide, and the next pulse was twice the width of the previous pulse. The last pulse was 200 times the width of the initial pulse. The sequence was repeated 10^5 times for a total duration of approximately 64 s. In Figure 5a, we compared the correlation of temperature versus time measured under −13 and −20 dBm microwave irradiation. The correlations are similar to their counterparts under CW irradiation, but the temperature rise is significantly reduced. The maximum rise at −13 and −20 dBm is 2.49 and 0.64 K, respectively. The temperature rise under higher irradiation is nearly 1 order larger than that under lower irradiation. The effect will cause the resonance frequency D_{gs} largely shift away from its original value.

Second, we studied the case of the general spin echo sequence. As shown in Figure 4b, the sequence consists of two $\pi/2$ pulses and an intermediate π pulse spaced by the free evolution time. The sequence was repeated 10^5 times for a total time of approximately 86 s. We compared the temperature time relations for −13 and −20 dBm microwave irradiation in Figure 5b, highly similar to CW irradiation and the Rabi pulse sequence, but the temperature rise was further reduced. The maximum temperature rise is 1.76 K for −13 dBm and 0.46 K for −20 dBm. The maximum temperature rise for −13 dBm is nearly 1 order larger than that for −20 dBm. Thus, the NV-diamond sensor will notably misread the true temperature of a target under microwave irradiation at −13 dBm.

Third, we investigated the case of a quantum lock-in XY8-N sequence, where N was taken to be 10. As shown in Figure 4c, the sequence consists of two $\pi/2$ pulses and 10 intermediate π pulses spaced by the free evolution time. The sequence was repeated 10^5 times for a total time of approximately 60 s. We compared the temperature time relations for −13 and −20 dBm microwave irradiation in Figure 5c. The maximum temperature rise is 0.07 K for −13 dBm and 0.03 K for −20 dBm. The temperature rise in both cases is negligible compared to those for the Rabi oscillation and the spin echo sequence.

4. CONCLUSIONS

In summary, our study demonstrates the existence of prominent microwave heating effect on the diamond sample, when reading the electronic ground triplet state of NV centers using ODMR based on continuous microwave, Rabi oscillation, or spin echo methods. The temperature rise induced by this effect is related to the irradiation power of the microwave and the process of generating the irradiation. For instance, for continuous microwave irradiation, Rabi oscillations, and spin echo methods, the temperature increment under −20 dBm irradiation varies between 16.16, 0.64, and 0.46 K. In contrast, the quantum-locked XY8-N pulse method produces a temperature rise of only 0.03 K. Considering that zero-field splitting D_{gs} is temperature-dependent, the microwave heating effect necessarily leads to a prominent redshift of D_{gs}. The microwave heating effect will inevitably perturb D_{gs} and the spin precession of the NV centers, leaving an NV-diamond sensor misreading the true temperature of target and perturbing magnetic field detection. Given bio-bodies including a significant amount of water, improper microwave irradiation may cause a large heating to the targets, or even kill the living cells. In all observations, the microwave heating effect is negligible for the quantum-locked XY8-N method.

AUTHOR INFORMATION

Corresponding Authors

Jintao Zhang − *National Institute of Metrology, Beijing 100029, China;* orcid.org/0000-0002-5204-3403; Email: zhangjint@nim.ac.cn

Xiaojuan Feng − *National Institute of Metrology, Beijing 100029, China*; Email: fengxj@nim.ac.cn

Authors

Zheng Wang − *Department of Precision Instrument, Tsinghua University, Beijing 100084, China; National Institute of Metrology, Beijing 100029, China*

Li Xing − *National Institute of Metrology, Beijing 100029, China*

Complete contact information is available at: https://pubs.acs.org/10.1021/acsomega.2c04232

Funding

This work was supported by the Fundamental Research Program of the National Institute of Metrology, China (nos. AKYZD2209-1 and AKYZD1904-2) and China Postdoctoral Science Foundation (no. 2021M703049).

Notes

The authors declare no competing financial interest.

ACKNOWLEDGMENTS

The authors greatly appreciate Dr. Gang. Q. Liu for generously sharing his expertized knowledge and the diamond NV samples.

REFERENCES

(1) Gruber, A.; Dräbenstedt, A.; Tietz, C.; Fleury, L.; Wrachtrup, J.; von Borczyskowski, C. Scanning Confocal Optical Microscopy and Magnetic Resonance on Single Defect Centers. *Science* **1997**, *276*, 2012−2014.

(2) Jelezko, F.; Wrachtrup, J. Read-out of single spins by optical spectroscopy. *J. Phys.: Condens. Matter* **2004**, *16*, R1089−R1104.

(3) Doherty, M. W.; Manson, N. B.; Delaney, P.; Jelezko, F.; Wrachtrup, J.; Hollenberg, L. C. L. The nitrogen-vacancy colour centre in diamond. *Phys. Rep.* **2013**, *528*, 1−45.

(4) Dobrovitski, V. V.; Fuchs, G. D.; Falk, A. L.; Santori, C.; Awschalom, D. D. Quantum Control over Single Spins in Diamond. *Annu. Rev. Condens. Matter Phys.* **2013**, *4*, 23−50.

(5) Schirhagl, R.; Chang, K.; Loretz, M.; Degen, C. L. Nitrogen-vacancy centers in diamond: nanoscale sensors for physics and biology. *Annu. Rev. Phys. Chem.* **2014**, *65*, 83−105.

(6) Wu, Y.; Liu, W. Q.; Geng, J. P.; Song, X. R.; Ye, X. Y.; Duan, C. K.; Rong, X.; Du, J. F. Observation of parity-time symmetry breaking in a single-spin system. *Science* **2019**, *364*, 878−880.

(7) Dolde, F.; Bergholm, V.; Wang, Y.; Jakobi, I.; Naydenov, B.; Pezzagna, S.; Meijer, J.; Jelezko, F.; Neumann, P.; Schulte-Herbruggen, T.; Biamonte, J.; Wrachtrup, J. High-fidelity spin entanglement using optimal control. *Nat. Commun.* **2014**, *5*, No. 3371.

(8) Waldherr, G.; Wang, Y.; Zaiser, S.; Jamali, M.; Schulte-Herbruggen, T.; Abe, H.; Ohshima, T.; Isoya, J.; Du, J. F.; Neumann, P.; Wrachtrup, J. Quantum error correction in a solid-state hybrid spin register. *Nature* **2014**, *506*, 204−217.
(9) Rose, B. C.; Huang, D.; Zhang, Z. H.; Stevenson, P.; Tyryshkin, A. M.; Sangtawesin, S.; Srinivasan, S.; Loudin, L.; Markham, M. L.; Edmonds, A. M.; Twitchen, D. J.; Lyon, S. A.; de Leon, N. P. Observation of an environmentally insensitive solid-state spin defect in diamond. *Science* **2018**, *361*, 60−63.
(10) Glenn, D. R.; Bucher, D. B.; Lee, J.; Lukin, M. D.; Park, H.; Walsworth, R. L. High-resolution magnetic resonance spectroscopy using a solid-state spin sensor. *Nature* **2018**, *555*, 351−364.
(11) Cujia, K. S.; Boss, J. M.; Herb, K.; Zopes, J.; Degen, C. L. Tracking the precession of single nuclear spins by weak measurements. *Nature* **2019**, *571*, 230−242.
(12) Staudacher, T.; Shi, F.; Pezzagna, S.; Meijer, J.; Du, J.; Meriles, C. A.; Reinhard, F.; Wrachtrup, J. Nuclear magnetic resonance spectroscopy on a (5-nanometer) ^{3} sample volume. *Science* **2013**, *339*, 561−563.
(13) Wolf, T.; Neumann, P.; Nakamura, K.; Sumiya, H.; Ohshima, T.; Isoya, J.; Wrachtrup, J. Subpicotesla Diamond Magnetometry. *Phys. Rev. X* **2015**, *5*, No. 041001.
(14) Wang, N.; Liu, G. Q.; Leong, W. H.; Zeng, H.; Feng, X.; Li, S. H.; Dolde, F.; Fedder, H.; Wrachtrup, J.; Cui, X. D.; Yang, S.; Li, Q.; Liu, R. B. Magnetic Criticality Enhanced Hybrid Nanodiamond Thermometer under Ambient Conditions. *Phys. Rev. X* **2018**, *8*, No. 011042.
(15) Kuwahata, A.; Kitaizumi, T.; Saichi, K.; Sato, T.; Igarashi, R.; Ohshima, T.; Masuyama, Y.; Iwasaki, T.; Hatano, M.; Jelezko, F.; Kusakabe, M.; Yatsui, T.; Sekino, M. Magnetometer with nitrogen-vacancy center in a bulk diamond for detecting magnetic nanoparticles in biomedical applications. *Sci. Rep.* **2020**, *10*, No. 2483.
(16) Tetienne, J. P.; Dontschuk, N.; Broadway, D. A.; Stacey, A.; Simpson, D. A.; Hollenberg, Lloyd. C. J. Quantum imaging of current flow in graphene. *Sci. Adv.* **2017**, *3*, No. e1602429.
(17) Toyli, D. M.; de las Casas, C. F.; Christle, D. J.; Dobrovitski, V. V.; Awschalom, D. D. Fluorescence thermometry enhanced by the quantum coherence of single spins in diamond. *Proc. Natl. Acad. Sci. U.S.A.* **2013**, *110*, 8417−8421.
(18) Kucsko, G.; Maurer, P. C.; Yao, N. Y.; Kubo, M.; Noh, H. J.; Lo, P. K.; Park, H.; Lukin, M. D. Nanometre-scale thermometry in a living cell. *Nature* **2013**, *500*, 54−59.
(19) Barry, J. F.; Turner, M. J.; Schloss, J. M.; Glenn, D. R.; Song, Y.; Lukin, M. D.; Park, H.; Walsworth, R. L. Optical magnetic detection of single-neuron action potentials using quantum defects in diamond. *Proc. Natl. Acad. Sci. U.S.A.* **2016**, *113*, 14133−14138.
(20) Miller, B. S.; Bezinge, L.; Gliddon, H. D.; Huang, D.; Dold, G.; Gray, E. R.; Heaney, J.; Dobson, P. J.; Nastouli, E.; Morton, J. J. L.; McKendry, R. A. Spin-enhanced nanodiamond biosensing for ultrasensitive diagnostics. *Nature* **2020**, *587*, 588−593.
(21) Kaminaga, K.; Yanagihara, H.; Genjo, T.; Morioka, T.; Abe, H.; Shirakawa, M.; Ohshima, T.; Kakinuma, S.; Igarashi, R. Non-contact measurement of internal body temperature using subcutaneously implanted diamond microparticles. *Biomater. Sci.* **2021**, *9*, 7049−7053.
(22) Lovchinsky, I.; Sushkov, A.; Urbach, E.; de Leon, N. P.; Choi, S.; de Greve, K.; Evans, R.; Gertner, R.; Bersin, E.; Müller, C.; McGuiness, L.; Jelezko, F.; Walsworth, R. L.; Park, H.; Lukin, M. D. Nuclear magnetic resonance detection and spectroscopy of single proteins using quantum logic. *Science* **2016**, *351*, 836−841.
(23) Sotoma, S.; Epperla, C. P.; Chang, H. C. Diamond Nanothermometry. *ChemNanoMat.* **2018**, *4*, 15−27.
(24) Liu, C. F.; Leong, W. H.; Xia, K.; Feng, X.; Finkler, A.; Denisenko, A.; Wrachtrup, J.; Li, Q.; Liu, R. B. Ultra-sensitive hybrid diamond nanothermometer. *Natl. Sci. Rev.* **2021**, *8*, No. nwaa194.
(25) Doherty, M. W.; Dolde, F.; Fedder, H.; Jelezko, F.; Wrachtrup, J.; Manson, N. B.; Hollenberg; Lloyd, C. L. Theory of the ground-state spin of the NV−center in diamond. *Phys. Rev. B* **2012**, *85*, No. 205203.
(26) Schwenke, A. M.; Hoeppener, S.; Schubert, U. S. Synthesis and Modification of Carbon Nanomaterials utilizing Microwave Heating. *Adv. Mater.* **2015**, *27*, 4113−4141.
(27) Neumann, P.; Jakobi, I.; Dolde, F.; Burk, C.; Reuter, R.; Waldherr, G.; Honert, J.; Wolf, T.; Brunner, A.; Shim, J. H.; et al. High-precision nanoscale temperature sensing using single defects in diamond. *Nano Lett.* **2013**, *13*, 2738−2742.
(28) Xie, T. Y.; Zhao, Z. Y.; Kong, X.; Ma, W. C.; Wang, M. Q.; Ye, X. Y.; Yu, P.; Yang, Z. P.; Xu, S. Y.; Du, J. F.; et al. Beating the standard quantum limit under ambient conditions with solid-state spins. *Sci. Adv.* **2021**, *7*, No. eabg9204.
(29) Lillie, S. E.; Broadway, D. A.; Dontschuk, N.; Scholten, S. C.; Johnson, B. C.; Wolf, S.; Rachel, S.; Hollenberg, L. C. L.; Tetienne, J. P. Laser Modulation of Superconductivity in a Cryogenic Wide-field Nitrogen-Vacancy Microscope. *Nano Lett.* **2020**, *20*, 1855−1861.
(30) Acosta, V. M.; Bauch, E.; Ledbetter, M. P.; Waxman, A.; Bouchard, L. S.; Budker, D. Temperature dependence of the nitrogen-vacancy magnetic resonance in diamond. *Phys. Rev. Lett.* **2010**, *104*, No. 070801.

https://doi.org/10.1021/acsomega.2c04232
ACS Omega 2022, 7, 31538−31543